

MINERALOGY OF EGYPTIAN BENTONITIC CLAYS I: DISCRIMINANT FUNCTION ANALYSIS

MOHAMED AGHA^{1,*}, RAY E. FERRELL², AND GEORGE F. HART²

¹ Department of Geology, Faculty of Science, Fayoum University, Egypt

² Department of Geology & Geophysics, Louisiana State University, Baton Rouge, LA, 70803, USA

Abstract—The purpose of the present investigation was to apply a discriminant function analysis (DFA) to quantitative mineralogical data from 124 Paleogene and Neogene bentonitic clays from the northern Western Desert of Egypt in order to establish an objective procedure for grouping the samples at three distinctly recognizable, but partially overlapping, levels of classification. These levels were province or geographic region, geologic age, and quarry. Quantitative mineralogical data were obtained by means of X-ray diffraction procedures employing least-squares fitting of simulated and standard mineral patterns with those from the laboratory. All data were transformed by a log-ratio procedure prior to the DFA. Fe-rich smectite (Fe_{oct}-1.4 a.p.f.u.), coarsely crystalline kaolinite, Fe-poor I-S (random with 60% S layers), quartz, and illite were the most important discriminator minerals. S-moderate I-S (random with 70% S), S-rich I-S (random with 80% S), two varieties of finely crystalline kaolinite, feldspar, and amorphous matter were also present. Calcite and gypsum were present in some samples. The median wt.% values for Fe-rich smectite, coarsely crystalline kaolinite, Fe-poor I-S, quartz, and illite in all samples were 16.6, 16.0, 15.2, 4.2, and 3.7, respectively. Abundances of quartz and feldspar have a good positive correlation, and finely crystalline kaolinite and Fe-rich smectite are negatively correlated. Other specific mineral associations are difficult to interpret visually because of the numbers of classes and variables employed in the investigation; however, DFA was successful in identifying statistically significant differences amongst the groups.

At the province level, the back-classification of the samples was successful 92% of the time at the highest probability level, or 100% if the first plus second probability results were utilized. For samples of the same age, 80% of the first-choice assignments were correct and >90% were correct when the second choice was included. At the quarry level, the predictability rate ranged from 76 to >90%. Using both probability results, only seven of the samples were misclassified. In a blind test of quarry samples, the DFA assignment was 80% correct. These tests confirm the objective reliability of class assignments based on DFA. Results based on this data set can be used to classify new samples in future geologic interpretations and economic exploitation of the deposits in the region.

Key Words—Bentonitic Clay, Clay Mineralogy, Discriminant Function Analysis, Egypt, Geographic Variability, Smectite.

INTRODUCTION

The mineralogical composition of clay-rich materials is a major factor in determining their geologic history or their physical and chemical behavior in industrial applications. In bentonites, for example, rheological behavior correlates with cation exchange capacity derived from the presence of abundant smectite (Odom, 1984; Ingelthorpe *et al.*, 1993). Variations in the relative abundance of smectite and the variety of associated minerals in clay deposits may occur on a microscopic scale within strata at the mesoscale within outcrops and quarries or the megascale of a single (or multiple) sedimentary basin(s). Geological factors producing the differences include climate, tectonic activity, types of rocks in the source terrane, transport processes,

characteristics of the depositional environment, diagenesis, metamorphism, and hydrothermal alteration (Galán, 2006). The geochemistry and mineralogy of a deposit may serve as a guide for the correlation and development of new commercial prospects and applications (Eisenhour and Brown, 2009).

Geochemical fingerprinting of K-bentonites using multivariate statistical analysis (Huff and Kolata, 1990) is one tool that has been employed successfully for regional (Christidis, 2001; Bertog *et al.*, 2007) and intercontinental correlation purposes (Huff *et al.*, 2010). Clusters of points on bivariate plots of geochemical parameters are one of the simplest ways to recognize differences amongst bentonites (Christidis, 2001), distinctive ash sequences in New Zealand (Moebis *et al.*, 2011), and Silurian K-bentonites in the Baltic region (Kiipli *et al.*, 2010). However, most cases do not present such simple solutions, and multivariate statistics offer a better analysis.

Mineralogical and geochemical data sets commonly contain multiple, complexly related variables that are

* E-mail address of corresponding author:

aliomaragha@yahoo.com

DOI: 10.1346/CCMN.2012.0600405

difficult to assign to classes or groups (*i.e.* based on age, environment, or location). Multivariate statistical procedures identify equations that provide for maximum separation amongst groups of variables based on two approaches. Principal component analysis (PCA), principal factor analysis (PFA), and various forms of cluster analysis seek to identify those variables that can be grouped into consistent classes that were not specified beforehand (Sanchez and Galán, 1995; Prudencio *et al.*, 2006; Ekosse and Mwitondi, 2009; Cravero *et al.*, 2010; Montero-Serrano *et al.*, 2010). Discriminant function analysis (DFA) identifies those functions that can be used to assign unknown samples to pre-existing classes (Hart *et al.*, 1989; Huff and Kolata, 1990; Hart, 1994; Shane and Froggatt, 1994; Kolata *et al.*, 1996; Ferrell *et al.*, 1998; Christidis, 2001; Eden *et al.*, 2001). In addition to fingerprinting for stratigraphic correlation or analysis of sedimentary environments, multivariate statistical methods have been applied to groups of minerals to establish their unique characteristics (Alberti and Brigatti, 1985; Galán *et al.*, 1998; Varadachari and Mukherjee, 2004).

The success of DFA for correlation and other geologic interpretations of geochemical fingerprinting is derived from its ability to assess subtle associations among large numbers of variables when the class has been identified by the investigator. The discriminant equations separate the variability amongst the groups and allow unknown samples to be classified with respect to group membership. Clustering and PFA methods are applied when the classes are unknown. An important consideration when applying multivariate statistics to compositional data is to transform the variables which may not have a normal abundance distribution to satisfy the assumption of multi-variable normality (Aitchison, 1986; Hart, 2011a).

The goal of the present report was to apply DFA to transformed mineralogical data from bentonitic clays in the northern Western Desert of Egypt to answer two fundamental questions that are critical to the interpretation of their origin and industrial utilization: (1) what are the mean mineral compositions and variability of the deposits? (2) How does the mineral content vary geographically and stratigraphically? The analysis will identify X-ray diffraction (XRD) predictor minerals and establish objective mineralogical characteristics that will be useful in establishing the differences among the deposits.

MATERIALS AND METHODS

Samples

Bentonitic clays, usually smectite-rich, are produced in four major mining districts (P1, P2, P3, and P4, Figure 1) including 12 quarries (numbered stars) in the northern Western Desert, south and west of Cairo, Egypt. In this presentation, bentonitic clay is used for

any soft, plastic, smectite-rich industrial clay regardless of its origin as recommended by Grim and Güven (1978) and Murray (2007). Local reports refer to the deposits as bentonites, but their derivation from volcanic materials is not clearly established. The deposits range in age from the Middle Eocene Epoch in the south to the Upper Pliocene Epoch in the north. The region around Fayoum (P4) is that which is mined most extensively. Bentonitic clay zones interstratified with siltstone, sandstone, or marly limestone vary in thickness from fractions of a meter to tens of meters. Typically the deposits are faintly laminated but more massive beds, or lenses, may occur. Fresh specimens generally are yellowish to greenish gray in color and have a waxy luster. Joints and other structures are frequently covered with Fe-oxyhydroxides. Smectite is the major clay mineral with accessory, or minor, illite and kaolinite. Weathering of Tertiary basalts and reworking by sedimentary processes in near-shore marine environments are implicated in the origin of the deposits (Abu El Ezz *et al.*, 1993). Beneficiated clay from some of the deposits has been evaluated for pharmaceutical and other applications (Hassan and Abdel-Khalik, 1998; Abdel-Motelieb *et al.*, 2011).

Sixty two samples of representative clay strata were collected from ~10–20 cm beneath the surface (Figure 1) from 12 quarry locations during 2009 (Table 1). Each sample was divided into two ~500 g portions to obtain replicate samples (A and B) for evaluation of small-scale sample variability at each location. A small, ~50 g block of each subsample was kept for scanning electron microscopy (SEM) and other analyses, while the remainder of the sample was crushed gently with a mortar and pestle to produce a coarse powder.

X-ray powder diffraction

Sample preparation. A representative portion of each sample (10 g) was obtained (using a sample splitter) for XRD analysis after additional gentle crushing. A 2 g aliquot designated for bulk mineralogy was ground in a Micronizer mill with ethanol for ~3 min to reduce the average particle diameter to ~5 μm . The powder dried at 60°C was side-loaded into an aluminum holder and scanned from 2 to 70°2 θ at 2.0 s per 0.02°2 θ step with a Siemens D5000 (Bruker) diffractometer in the reflection mode utilizing a Cu tube operated at 40 kV and 30 mA.

The other aliquot (8 g) was used to obtain the clay-sized fraction by gravity settling. Samples were dispersed in a 0.01% Na₃PO₄ solution and left undisturbed for 3.5 h, after which the top 5 cm was siphoned off (the <2 μm fraction) and concentrated by high-speed centrifugation at 12500 rpm giving a relative centrifugal force (RCF) of 18168 \times g for 35 min. After decanting the supernatant liquid and homogenization of the clay paste, an oriented clay aggregate was prepared by smearing on a glass slide. The slides were scanned between 2 and 36°2 θ with the same operating conditions as indicated

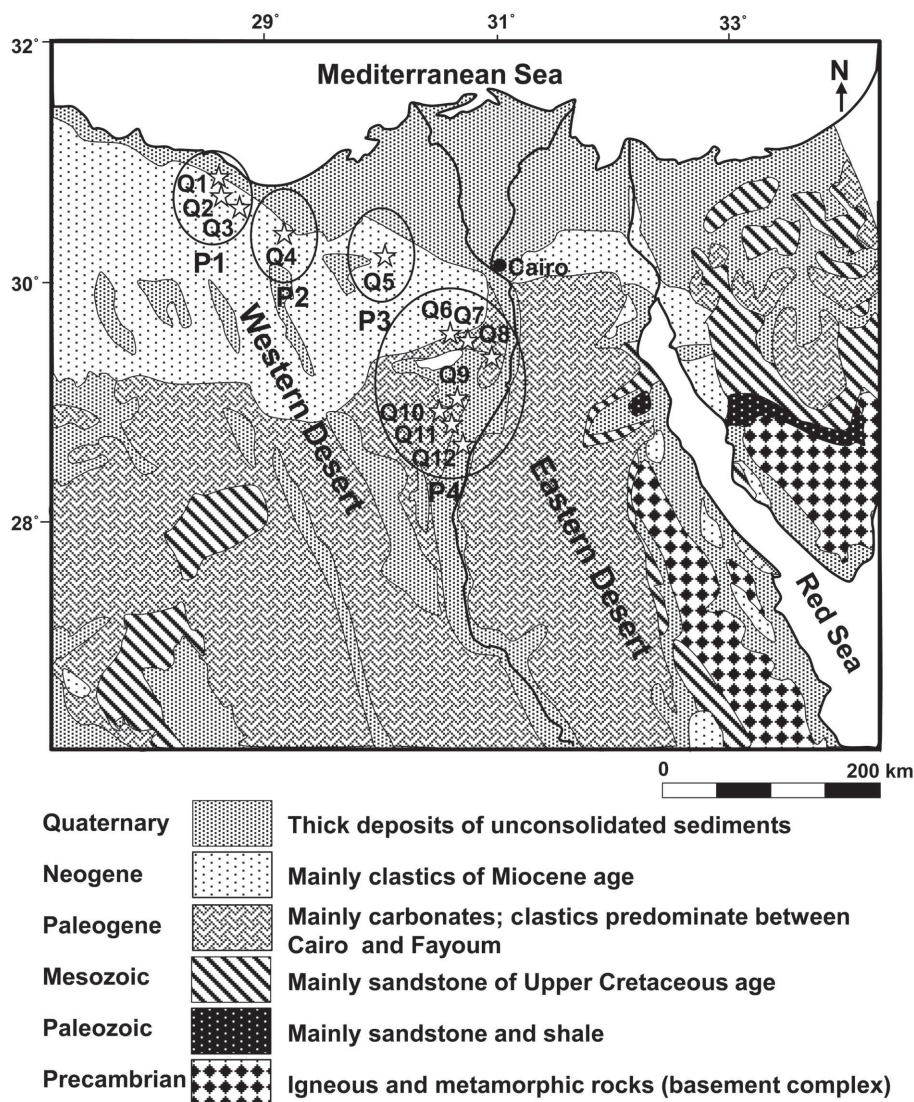


Figure 1. Approximate locations of quarries (numbered stars) in the northern part of the Western Desert of Egypt. P1, P2, P3, and P4 indicate the province. More detailed sample-site information is presented in Table 1.

Table 1. Province, quarry name, and age of bentonite sampling sites in the Western Desert of Egypt.

Province	Quarry	Age (epoch)
P1, south of Alamein city	Q1, Deir El Moreir	Middle Miocene
P1, south of Alamein city	Q2, Deir Abul Hegif	Middle Miocene
P1, south of Alamein city	Q3, Deir El Harrah	Middle Miocene
P2, south of El Hammam city	Q4, El Barkan	Lower Miocene
P3, Wadi El Natrun Valley	Q5, Deir El Baramous	Upper Pliocene
P4, El Fayoum Depression	Q6, Qasr El Sagha	Upper Eocene
P4, El Fayoum Depression	Q7, Kom Oshim	Upper Eocene
P4, El Fayoum Depression	Q8, Girza	Middle Eocene
P4, El Fayoum Depression	Q9, Qalamshah	Middle Eocene
P4, El Fayoum Depression	Q10, Cemetery	Unknown
P4, El Fayoum Depression	Q11, Shaklofa	Middle Eocene–Upper Pliocene
P4, El Fayoum Depression	Q12, Reigha	Unknown

above. The samples were run after air-drying, after saturation with ethylene glycol for at least 16 h at room temperature, and after heating for 1 h at 300 and 550°C.

Whole-sample XRD analysis. Whole-sample mineral identification was carried out by matching observed d values with those in the *MacDiff* 4.2.5 database (Petschick, 2004) after peak correction using the 3.34 Å quartz (101) peak. Quantitative estimates of the amounts of quartz, feldspars, calcite, gypsum, and total clay minerals were obtained by multiplying the integrated peak area of distinctive peaks by the mineral intensity factors reported by Cook *et al.* (1975); except that the total clay-mineral peak intensity factor was increased to 20 according to Ferrell *et al.* (1998). The precision of the technique is ± 10 –15% at the 10 wt.% level.

Clay-fraction mineralogy. Qualitative analysis of the clay fraction was accomplished by tabulating the mineral peaks on the air-dried, ethylene glycol-saturated, 300°C and 550°C heated patterns and noting their response to each treatment. The quantitative interpretation procedures were similar to those described by Ferrell and Dypvik (2009), where observed ethylene glycol patterns and simulated *Mulcalc* patterns (Aparicio and Ferrell, 2001) are matched using the whole-pattern, least-squares method in *CLAY++* (Ferrell, 2006). By adjusting fractional multipliers, the *CLAY++* program matches composite synthetic pattern intensities created by *Mulcalc* 1.0 with actual glycolated pattern intensities at each data point in the XRD pattern. Finally, the

CLAY++ percentages were multiplied by the total clay values to obtain their representative weight percentages in the whole-rock sample. The results are quantitative representations (QR) of percentage clay mineral content with an approximate precision of $\pm 10\%$, and are not strictly weight percentage values.

The simulation parameters used to produce the synthetic standard patterns included: layer type, octahedral sheet Fe content, interlayer cations, crystallite size distribution, and stacking sequences. The Fe content in the smectite (Dis, or dioctahedral smectite) and mica/illite layers (Dim, or dioctahedral mica) was determined by trial and error matching of computed patterns with 0–2 Fe atoms in the octahedral sheet. The best ‘fit’ was obtained with 1.4 Fe atoms in the Fe-rich smectite and no Fe in the I-S smectite layers. The Fe content and b -axis dimensions of the Fe-rich smectite were similar to an Fe-montmorillonite from the Northern Territories of Australia (Eggleton, 1977). The fractions of smectite layers in Fe-poor I-S, S-moderate I-S, and S-rich I-S were 0.6, 0.7, and 0.8, respectively. All the stacking sequences were random, $R = 0$. The mineral name, XRD filename, and parameters for each reference pattern are listed in Table 2. Actual XRD patterns were used for both quartz and kaolinite after adjusting for differences in mineral intensity factors. The quantity of amorphous material was estimated by calculating the fractional multiplier for the XRD pattern of a glass slide. A complete table of all XRD results is available from the corresponding author. The ‘Goodness of fit index’ or RR values ranging between 0.007 and 0.029, all below 0.05,

Table 2. Minerals used in a quantitative XRD matching routine.

Mineral	XRD file name	Simulation parameters
Fe-rich smectite	FeDISM	Pure 2EG-Dis: Dis Fe = 1.4. Defect broadening; mean defect-free distance = 3; high $N = 5$.
Fe-poor I-S	DISM3/IL	0.6 2EG-Dis: Dis Fe = 0 + 0.4 Dim: K = 0.9. Defect broadening; mean defect-free distance = 3; high $N = 5$, $R = 0$.
S-moderate I-S	DISM2/IL	0.7 2EG-Dis: Dis Fe = 0 + 0.3 Dim: K = 0.9. Defect broadening; mean defect-free distance = 3; high $N = 5$, $R = 0$.
S-rich I-S	DISM1/IL	0.8 2EG-Dis: Dis Fe = 0 + 0.2 Dim: K = 0.9. Defect broadening; mean defect-free distance = 3; high $N = 5$, $R = 0$.
Illite	ILLITE	Pure Dim: Dim K = 0.9. Defect broadening; mean defect-free distance = 7; high $N = 40$.
Finely crystalline kaolinite	K1	Pure kaolinite. Defect broadening; mean defect-free distance = 7; high $N = 35$
Kaol2	K2	Actual XRD pattern (finely crystalline)
Coarsely crystalline kaolinite	K3	Actual XRD pattern used for whole-rock and clay-fraction analysis
Quartz	Clay-sized Qz	Actual XRD pattern
Glass	Amorphous	Glass slide XRD pattern
Feldspar	Feld	Actual XRD pattern
Calcite	Cal	Actual XRD pattern
Gypsum	Gyp	Actual XRD pattern

All patterns are normalized to quartz intensity of 2000 counts. K – kaolinite; I-S – mixed-layer illite-smectite; S – smectite; Dis – dioctahedral smectite; EG – ethylene glycol saturated; Dim – dioctahedral mica; N – number of crystallites; R – Reichweite or ordering index.

indicate an acceptable match between the actual EG XRD pattern and the simulated composite pattern for all samples (Ferrell and Dypvik, 2009).

Statistical analysis methods

The XRD data frames are closed arrays that sum to 100% and thereby suffer from the closure problem typical of compositional data when subjected to multivariate statistical analyses requiring a multi-normal distribution (Chayes, 1960; Aitchison, 1986; Weltje, 2002; von Eynatten *et al.*, 2003; Daunis-I-Estadella *et al.*, 2006; Martin-Fernandez and Thio-Henestrosa, 2006; Barbera *et al.*, 2009). The problem originates because closed arrays of XRD percentages are within simplex space (S) and have values ranging from 0 to 100% (or 0 to 1), but classical statistics works within real-number space, which has a range of minus infinity to plus infinity. Aitchison (1986) developed some procedures that are applicable to percentage data that involve a log-ratio transformation to convert the vector from simplex space to real-number space. The present study used a log-ratio transformation in which feldspar wt.% was used as the divisor. Because log transformations cannot handle zero values, but the lower limit of detection of XRD-derived variables can be calculated for each variable, a suitable substitute is 0.05 wt.%. This value was used for all phases.

Selection of variables for multivariate analysis.

Extensive statistical tests (Hart, 2011b) were applied to the data frame prior to multivariate analysis to select the predictor variables to be used in the DFA. Each variable in the data frame was examined for normality by the eye-

ball method using box plots, followed by a test for skewness, kurtosis, a P-P plot (percent-percent), and calculation of the Shapiro-Wilk test (Shapiro and Wilk, 1965) for normality. The R statistical package v.2.10.1 (2009) was used for the DFA.

RESULTS

Qualitative mineral content

A composite pattern produced by adding intensities from six calcite-free sample patterns from quarry Q1 (Figure 2) contained peaks produced by expandable clay mineral(s) with 15–12 Å d values (5.92 – $7.34^{\circ}2\theta$), mica (illite plus muscovite) at 10 Å ($8.86^{\circ}2\theta$), and kaolinite or chlorite at 7.2 Å ($12.28^{\circ}2\theta$). The total clay peak (TC) near 4.5 Å ($20^{\circ}2\theta$) represents all phyllosilicates present. Quartz (Qz) is represented by peaks at 4.26 Å ($20.84^{\circ}2\theta$) and 3.34 Å ($26.66^{\circ}2\theta$). Small peaks ranging from 3.25 to 3.19 Å (27.45 – $27.95^{\circ}2\theta$) are attributed to one or more members of the feldspar group. The remaining peaks represent additional reflections from minerals above. The d_{060} reflections between 1.49 and 1.50 Å (62.14 – $61.96^{\circ}2\theta$) indicate the presence of dioctahedral montmorillonite in all samples. Some samples from quarries Q6, Q8, Q10, and Q12 in El Fayoum Province (P4) contain calcite.

The XRD patterns for the clay-sized fraction ($<2\ \mu\text{m}$) of a representative sample following air-drying (AD), ethylene glycol saturation (EG), 300°C heating (300), and 550°C (550) heating (Figure 3) revealed the presence of smectite by the shifting of the air-dried 12.9 Å ($6.8^{\circ}2\theta$) broad peak to ~ 16.93 Å ($5.22^{\circ}2\theta$) after saturation with ethylene glycol and its collapse after

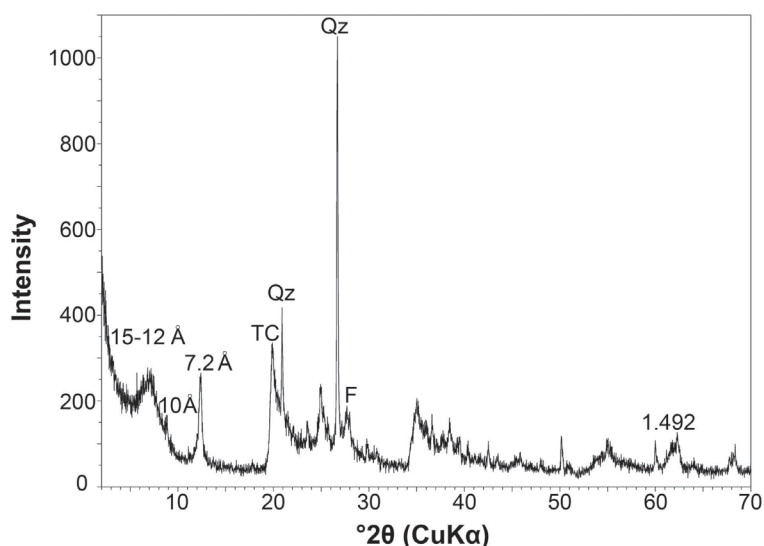


Figure 2. Representative composite XRD pattern produced by adding six XRD patterns for randomly oriented powders of calcite-free samples from quarry Q1 in province P1. The d values of the peaks are numbered. TC = total clay; Qz = quartz; F = feldspar. The dioctahedral nature of the clays is indicated by the 1.492 Å peak.

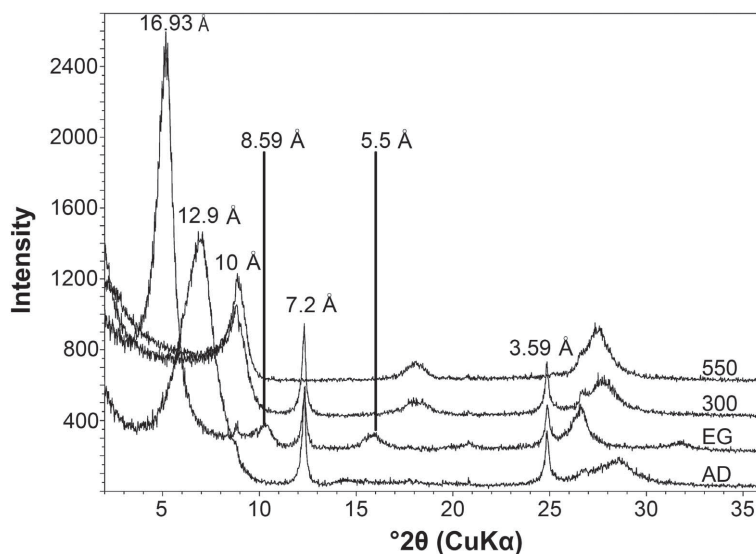


Figure 3. XRD patterns for sample s015 indicating the changes produced by various treatments of the oriented clay fraction sample. AD = air dried; EG = ethylene glycol saturated; 300 = heated at 300°C for 1 h; 550 = heated at 550°C for 1 h. The d values of the peaks are numbered. Qz = quartz.

heat treatments to ~ 10 Å ($8.8^\circ 2\theta$). The presence of illite was established by the small 10 Å ($8.8^\circ 2\theta$) peak in both AD and EG patterns. The increased intensity of the 10 Å peak after heating is due to the superposition of collapsed smectite layers. Kaolinite was identified by the symmetrical, sharp, and relatively high-intensity 7.2 Å ($12.3^\circ 2\theta$) peak and the higher order reflections at 3.59 Å ($24.8^\circ 2\theta$) and 3.38 Å ($26.38^\circ 2\theta$) that did not change during the EG and 300°C treatments, but are destroyed with the 550°C treatment. None of the samples showed any indication of chlorite. Unlabeled peaks are other reflections from the minerals identified above. The only non-clay mineral detected in the clay-sized fraction was quartz (Qz).

The intense, broad peak near $5.2^\circ 2\theta$ (17 Å) on EG samples often produced a non-integral series of peaks. The coefficient of variation (CV) values for the mean smectite-rich peaks exceed the 0.75% minimal value required to establish the presence of mixed-layered materials (Bailey, 1982). In addition, the angular differences between the mostly 002 and 003 reflection positions ($\Delta 2\theta$) are indicative of random interlayered illite-smectite with 70–75% smectite layers (Moore and Reynolds, 1989; Środoń, 2006). The observed $\Delta 2\theta$ (5.92°) and the CV (3.40%) are close to the values produced by the simulated pattern for a randomly interstratified illite-smectite containing 80% smectite layers (S-rich I-S). The variability of the XRD patterns reveals a more complex mineral assemblage than is typical for smectite-rich bentonitic clays.

The d_{001} smectite values obtained at laboratory relative humidity conditions by all but three of the AD samples ranged between 12.6 and 13.6 Å. The mean value of 12.9 Å suggests that Na was the dominant

interlayer cation. However, relative humidity differences and interlayering between smectite and illite can cause peak shifting that can lead to misinterpretation of the smectite exchangeable ions. Actual measurements of the exchangeable cations were complicated by the presence of halite, gypsum, and calcite. Preliminary CEC data for samples with minimal amounts of soluble species confirmed the dominance of exchangeable Na.

Quantitative X-ray mineralogy

The most abundant minerals (Table 3) with median values >15 wt.% included Fe-rich smectite, finely crystalline kaolinite, coarsely crystalline kaolinite, and randomly ordered mixed-layered I-S with 0.6 smectite layers (Fe-poor I-S). The median (med.), first quartile (q1), and third quartile (q3) abundance values were highly variable, ranging, for example, from 5 to 45 wt.% for the Fe-rich smectite. Amorphous (Amph) substances had a median close to 7 wt.% and a wide range of abundance from 21 to 2.5 wt.%. The least abundant minerals had medians of <5 wt.% and are represented by a second kaolinite (KAOL2), illite, quartz, S-moderate I-S, S-rich I-S, feldspars (Feld), calcite (Cal), and gypsum (Gyp). Calcite and gypsum were absent from many of the samples. Quartz, calcite, gypsum, Fe-rich smectite, amorphous matter, finely crystalline kaolinite, KAOL2 (finely crystalline sample from Georgia), and S-moderate I-S distributions were positively skewed while coarsely crystalline kaolinite, illite, and S-rich I-S values were negatively skewed. The highly skewed results supported the need to transform the variables prior to multidimensional statistical analyses.

Quartz and feldspar; Fe-rich smectite and amorphous matter (Amor); Fe-rich smectite and finely crystalline

Table 3. Summary of mineral abundances in all samples of Egyptian bentonite.

Summary statistics	Quartz	Feldspar	Calcite	Gypsum	Fe-rich smectite	Illite	Amorphous	KAOL2	Coarsely crystalline kaolinite	Finely crystalline kaolinite	S-moderate I-S	S-rich I-S	Fe-poor I-S	Clay-sized quartz
q1	2.7	1.1	0.0	0.0	10.4	2.2	5.5	2.6	12.5	13.1	1.7	1.5	11.8	0.0
Min	1.2	0.7	0.0	0.0	4.8	2.0	2.7	0.0	4.2	4.5	0.0	0.0	4.4	0.0
Median	4.2	1.7	0.0	0.0	16.6	3.7	6.8	4.6	16.0	17.8	3.1	2.3	15.2	0.0
Max	11.4	5.9	8.3	0.4	45.0	12.6	21.3	13.5	25.5	37.6	11.7	5.7	36.0	3.0
q3	6.2	2.3	1.8	0.0	28.8	4.4	8.9	7.1	18.2	26.2	6.1	3.0	18.7	1.2

KAOL2 finely crystalline kaolinite
 q1 = first quartile; Min = minimum; Max = maximum; q3 = third quartile

kaolinite; and amorphous matter and coarsely crystalline kaolinite are co-dependent variables (Figure 4). The ‘null’ hypothesis that the variables were not related was rejected at the 95% percent confidence level. A positive correlation existed between quartz and feldspar, and between amorphous substances and Fe-rich smectite. On the other hand, Fe-rich smectite and finely crystalline kaolinite, and amorphous substances and coarsely crystalline kaolinite showed negative correlations. The four relationships suggested in the scatter-plots exhibited highly significant correlations ($p < 0.05$), but the quality of the adjusted R^2 ranges from good (0.662) to poor (0.215).

The outcome of the initial statistical appraisal of the distribution of the individual variables was a rejection table that helped to identify a smaller number of predictor variables to be used in the analysis (statistical pre-processing). The acceptance/non-acceptance decisions for the original 14 XRD variables are summarized below:

(1) The analysis of All (the complete data frame) is, geologically, not very relevant to the present study and, therefore, little weight is attached to its values in the rejection table.

(2) Analyses of the provinces’ data frames have geological significance for any regional interpretation.

(3) Analyses of the quarry data frames are of principal interest in the study.

(4) Clay-sized quartz (Cq), gypsum (G), amorphous (A), and calcite (C) were removed immediately from the analysis, mostly because of their absence from a large number of samples.

(5) The scatter plots for co-dependency (Figure 4) showed linkage between quartz and feldspar, Fe-rich smectite and amorphous material, and Fe-rich smectite with finely crystalline kaolinite, all of which suggest that quartz and Fe-rich smectite should be kept and the other correlated variables (finely crystalline kaolinite and amorphous matter) dropped.

(6) Statistical tests for skewness, normality, and variance-covariance assumptions identified seven predictor variables suitable for multivariate analysis of the data frame: quartz, Fe-rich smectite, illite, finely crystalline kaolinite (KAOL2), coarsely crystalline kaolinite, S-moderate I-S, and Fe-poor I-S. These seven variables were used to relate mineral-abundance changes to province, age (Epoch), and quarry.

Characteristics of the provinces

The number of XRD predictor variables available for the DFA at the province level is seven; the number of classes, provinces, is four; and the smallest N , number of samples, is eight, allowing three linear discriminant functions (LD) to be generated. The largest absolute loading values in each of the functions are associated with Fe-rich smectite, coarsely crystalline kaolinite, quartz, and Fe-poor I-S, making them the most important predictors of variability at the province level.

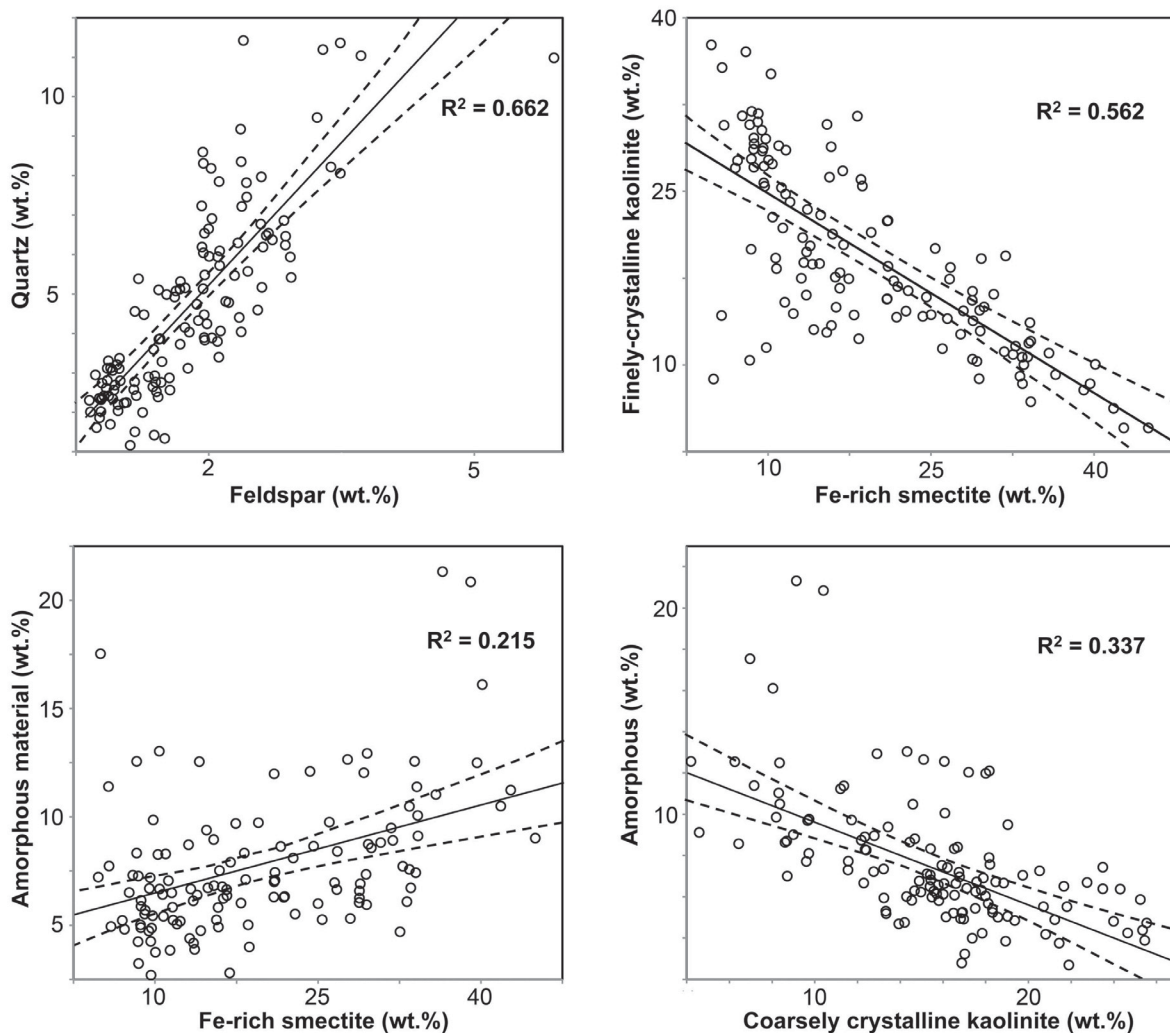


Figure 4. Pair plots of selected XRD variables (wt.%). Line of linear best-fit to data and R^2 shown in each frame.

The scatter of linear discriminant function 1 (LD1) and linear discriminant function 2 (LD2) values (Figure 5) provides evidence that P2 and P3 are easily distinguished from one another and from P4 and P1. Large positive values of LD1 and LD2 are present in P2, while P3 is characterized by high values of LD1 and negative LD2 values. Although P1 and P4 data points produce mostly distinct clusters on the graph, they have some overlap. Seven P1 samples plot within the P4 field and one P4 result plots within the P1 field. The first discriminant function (LD1) accounts for 57.2% of the variation and the second discriminant function (LD2) for 40.35% of the variation seen in the provinces. LD3 accounts for only a minor amount (2.44%) of the variability.

When each sample was back-classified into the predicted class, good predictability was observed. Of the 124 samples, only 10 (8%) were misclassified. The second choice for the ten samples, the next highest

probability of class membership, turned out to be the correct classification. The ability to assign samples to a particular class based on probability estimates of membership represents a major advantage of DFA. In characterizing the variability in the provinces using descriptive statistics, those samples that were incorrectly classified using the DFA were eliminated and the reduced (purified) data frame used to provide a 'tighter' view of the mineral variability within each province.

Fe-rich smectite has the greatest variation in median abundance in samples at the province level (Figure 6a). P2 samples have a median value of 39.1 wt.%, three to four times greater than in the other provinces (8.7 to 17.9 wt.%), and its range is mostly free of overlap. The other important smectite-containing mineral, Fe-poor I-S (Figure 6b), is most abundant in P3 (28.3 wt.%) and the spread of its median values, 14.5 to 28.3 wt.%, is not as great as for Fe-rich smectite. Coarsely crystalline kaolinite (Figure 6c) falls into two groups: the P1 and

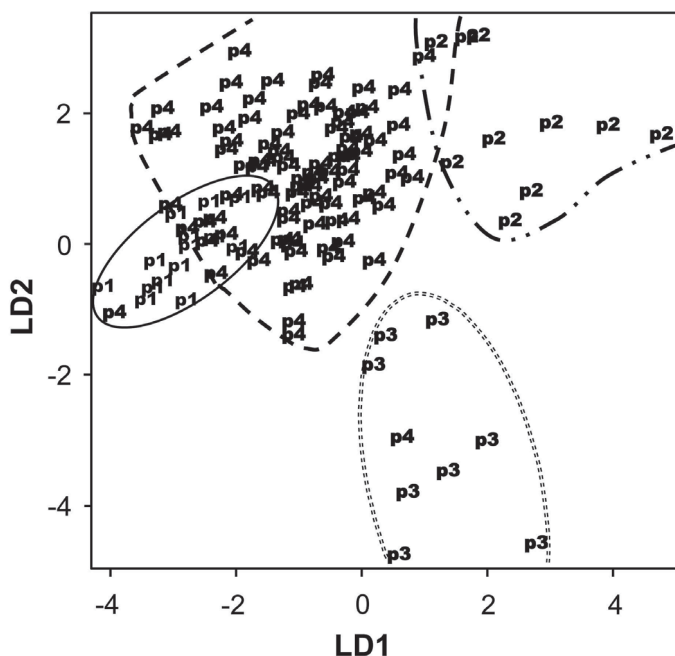


Figure 5. Scatter plot of LD1 and LD2 results at the province level. Lines have been drawn to outline fields that are mostly free of overlap.

P4 samples have median values between 15 and 20 wt.% while P2 and P3 medians are <10 wt.%. Quartz (Figure 6d) is the least important of the four province predictor variables. It is the least abundant mineral in all provinces and its values in all locations overlap.

Characteristics of the epochs

The age of ten unknown samples from quarries Q10 and Q12 was predicted with a preliminary DFA employing seven XRD predictor minerals and five age classes. The smallest number of samples per class was 10. Quarry 12 samples were all assigned to the Upper Eocene Epoch and those from Q10 were assigned to the Lower Miocene Epoch (with the second choice as Upper Eocene Epoch) or the Upper Eocene Epoch (with the second choice Middle Eocene Epoch). Samples from Q10 exhibited minimal affinity with the Middle Miocene Epoch samples and no affinity with the Pliocene Epoch samples.

After adding the predicted age samples to the data frame, a new DFA for Epochs was run. Five distinct fields (territories) were revealed in the scatter-plot of LD1 vs. LD2 for Epochs (Figure 7). The Lower Miocene and Pliocene Epoch samples are readily distinguished on the basis of high and moderate LD1 values, and low vs. high values for LD2, respectively. Results for the other age samples also plot within distinct clusters, although with moderate overlap.

The LD1 accounts for 59.8% of the variance and LD2 for 33.7%, a total of 93.5% of the variance seen in the distribution of the samples by Epoch. Fe-rich smectite, Fe-poor I-S, coarsely crystalline kaolinite, illite, and

quartz are the main contributors to LD1 and LD2. When each sample was back-classified into the predicted Epoch, samples from Q10 and Q11 were misclassified. Of the 124 samples, 26 were misclassified (22%) and the second choice for class was the correct one in 21 cases (96% correct). The samples that were incorrectly classified using the DFA were eliminated in subsequent calculations of the descriptive statistics relating mineral content to age.

The general distribution of Fe-rich smectite at the Epoch level (Figure 8a) is similar to the pattern at the province level. One class (L. Miocene) has a high median that is almost four times greater than in the lowest class (U. Miocene). The Fe-rich smectite median values are ~10 wt.% (M. Miocene and Pliocene), 14.8 wt.% (M. Eocene), 21 wt.% (U. Eocene), and 37.8 wt.% (L. Miocene). The values are positively skewed in all Epochs, except the M. Eocene. The M. Miocene samples have a very narrow abundance range for Fe-rich smectite that can be partially separated from U.- and M.-Eocene ones. Fe-poor I-S (Figure 8b) and illite (Figure 8e) abundances in the Pliocene class are distinguished from other classes by their high values. Quartz is least abundant with overlapping distributions (Figure 8d). The complexities of these associations and the large number of variables underscore the need for a multivariate statistical approach to classification. Geological conditions in the L. Miocene favored the formation of Fe-rich smectite deposits while optimal conditions for coarsely crystalline kaolinite accumulation were attained in the U. Eocene and M. Miocene. The largest quantity of Fe-poor I-S occurs in Pliocene

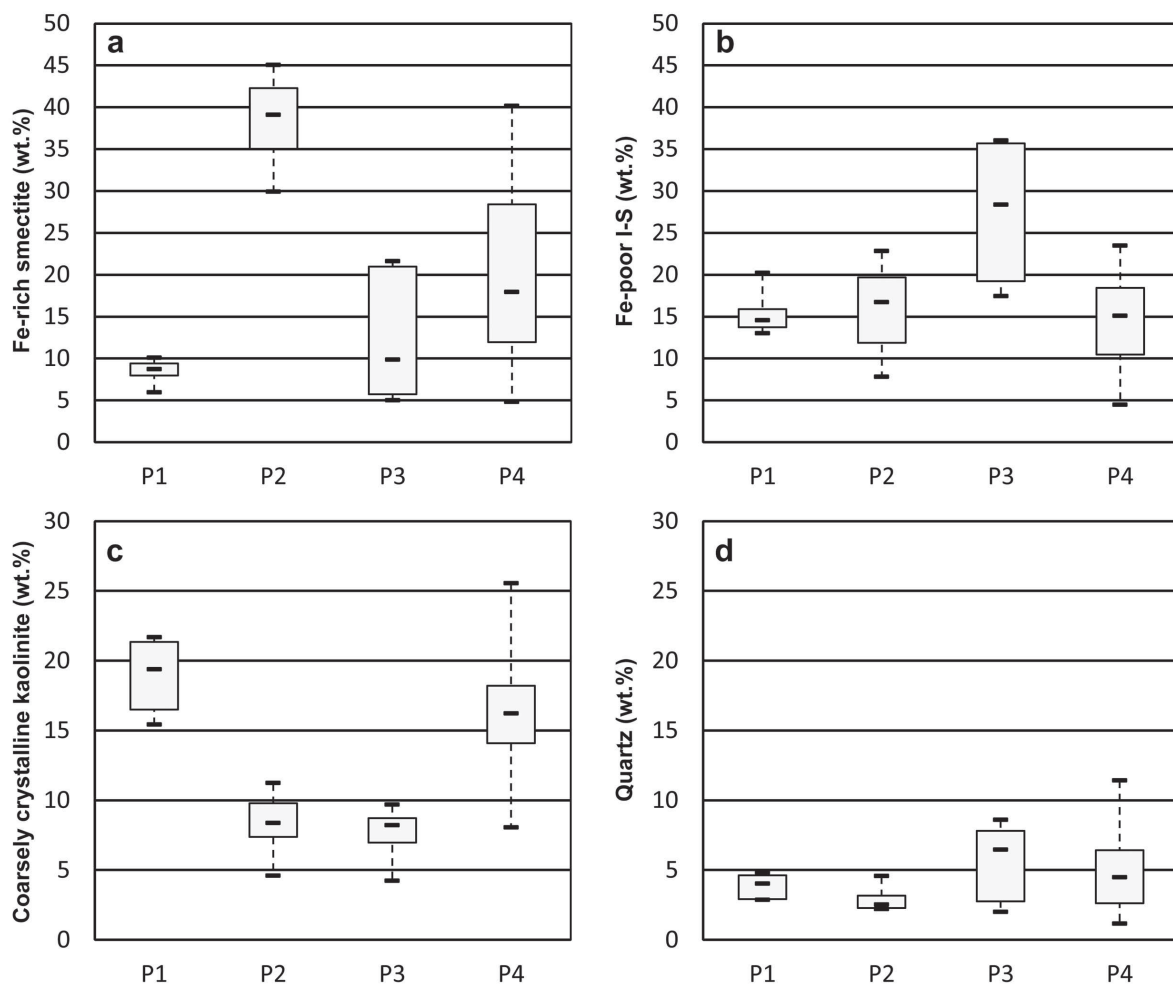


Figure 6. Box plot of XRD predictor-mineral abundances in each province based on class assignments derived from a modified DFA model. Values are given in Table 4.

sediments. Events favoring the development of these differences are discussed in a companion paper on the genesis of the Egyptian bentonitic clays (Agha *et al.*, in revision).

Characteristics of the quarries

At this level of investigation, the number of classes is 12 and the smallest N value is 2 (Q10). Only seven XRD predictor variables are present so the maximum number of classes (quarries) had to be reduced from 12 to 7 and the smallest N ($= 2$) had to be increased prior to DFA. Study of the Epochs suggests that data from quarries Q1, Q2, and Q3 can be agglomerated as Qc because they are all of the same age and similar in composition (now, $N = 14$). The two quarry 10 results for the age classification were problematic and were dropped from further analysis. Quarries Q5 and Q11 are both Pliocene and are agglomerated (now with the expanded Q5, $N = 12$). Quarries Q7 and Q12 are both Upper Eocene and are agglomerated as data set Qf (N is

now = 26). Thus, the number of classes has been reduced to seven and the number of members in the classes has increased.

From the overlapping of the LD1 values (x axis, Figure 9), some quarries clearly will not separate out easily on the basis of a single function, except for Q4. When LD1 and LD2 values are considered, the separation of Q4 is clearer and, although intermingling occurred, the other quarry results tend to occur in separate zones (Figure 9). LD1 accounts for 65% of the discrimination, LD2 for 16.6% and LD3 for 12.4%, with the sum of the other three discriminant functions accounting for ~5.4%. Only the first two functions are considered, as they account for much of the variability. The predictors with the greatest power of discrimination, *i.e.* largest loading values, are Fe-rich smectite, coarsely crystalline kaolinite and Fe-poor I-S in LD1, and coarsely crystalline kaolinite and illite in LD2.

When each sample was back-classified into the predicted class, 30 of the 122 samples were misclassified

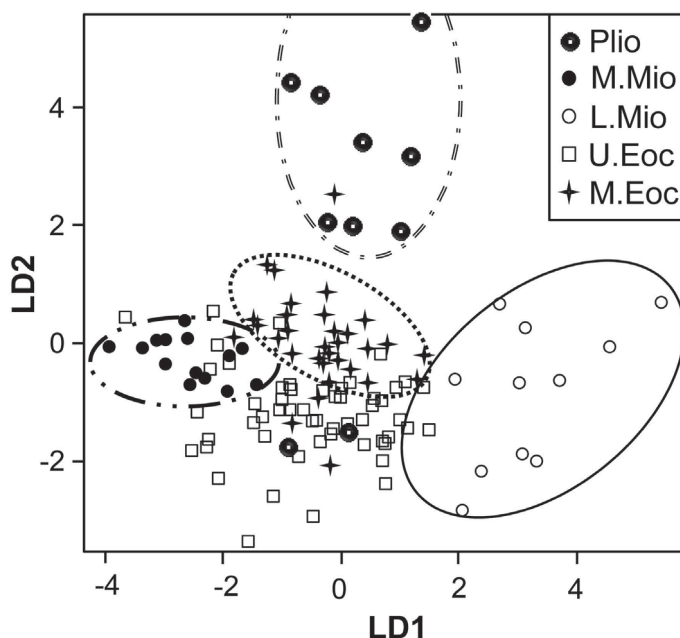


Figure 7. Scatter plot of LD1 and LD2 results at the Epoch (age) level. Lines have been drawn to outline fields that are mostly free of overlap.

(24.6%), but the second choice for class was correct for 23 of them, raising the acceptance level to 94%. This is considered a good result considering the type of data frame analyzed, *i.e.* compositional. Using the DFA, the probability that a sample could be assigned to the quarry of origin based on its mineral content is 75–94%.

At the quarry level (Figure 10), compositional values exhibit some of the same differences described above, but more detail is revealed because of the larger number of classes. The quarries are arranged according to their age, starting from the left with the youngest one (Q5; Upper Pliocene) in order to facilitate visual comparison

Table 4. Summary statistics for predictor minerals at the province level. Values in wt.%.

Mineral predictor	Statistical parameters	P1	P2	P3	P4
Fe-rich smectite	min	6.0	29.9	5.0	4.8
	max	10.1	45.0	21.6	40.1
	median	8.7	39.1	9.8	17.9
	q1	8.0	35.0	5.7	12.0
	q3	9.4	42.3	21.0	28.4
Coarsely crystalline kaolinite	min	15.4	4.6	4.2	8.0
	max	21.7	11.2	9.7	25.5
	median	19.4	8.4	8.2	16.2
	q1	16.5	7.4	7.0	14.1
	q3	21.3	9.8	8.7	18.2
Fe-poor I-S	min	13.0	7.8	17.4	4.4
	max	20.2	22.8	36.0	23.5
	median	14.5	16.7	28.3	15.1
	q1	13.7	11.9	19.2	10.5
	q3	15.9	19.7	35.7	18.4
Quartz	min	2.9	2.2	2.0	1.2
	max	4.8	4.6	8.6	11.4
	median	4.0	2.5	6.5	4.5
	q1	2.9	2.3	2.8	2.6
	q3	4.6	3.2	7.8	6.4

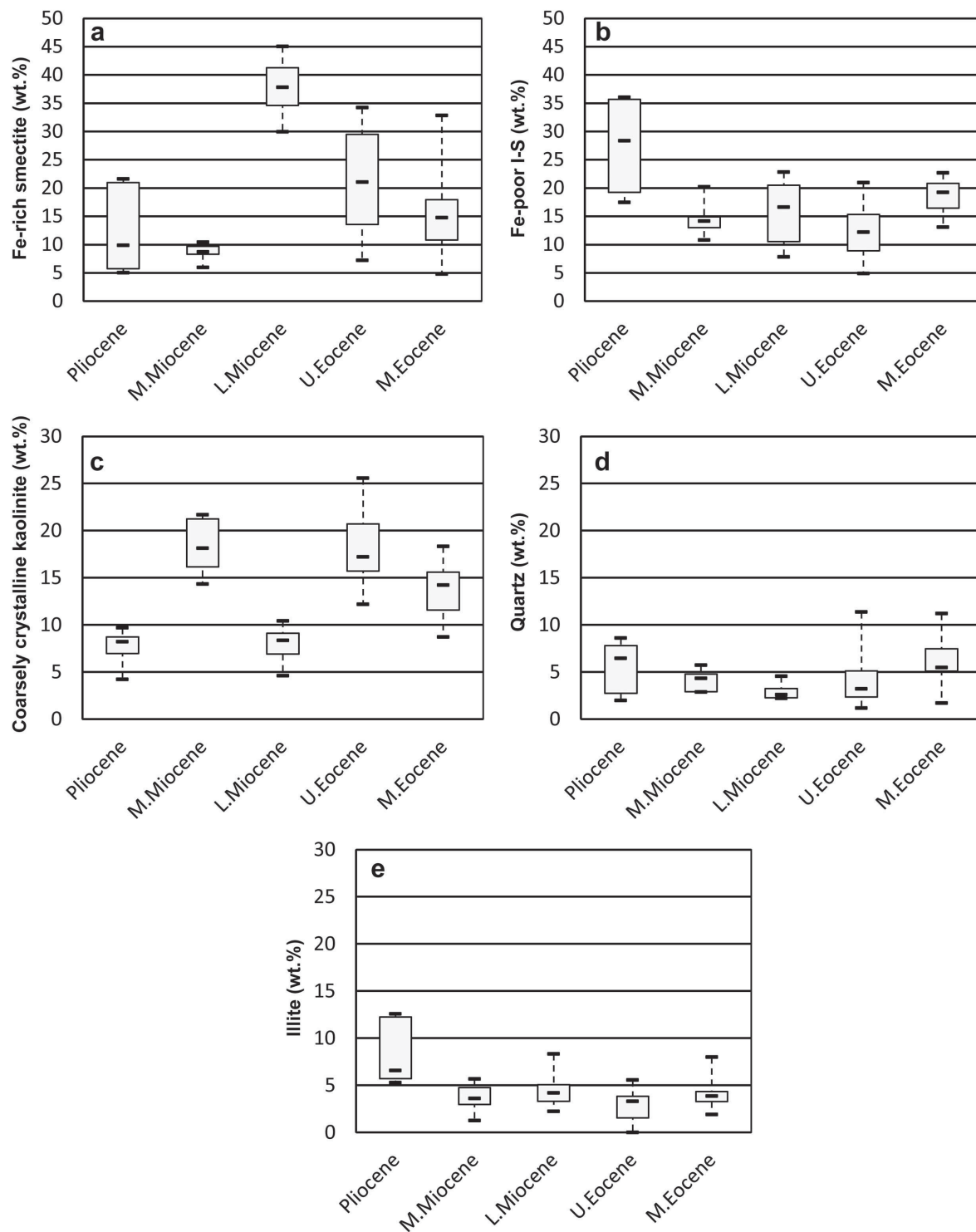


Figure 8. Box plot of XRD predictor-mineral abundances in each Epoch (age) class based on class assignments derived from a modified DFA model. Values are given in Table 5.

with the Epoch data (Figure 8). Fe-rich smectite (Figure 10a) and Fe-poor I-S (Figure 10b) medians are distinctly higher than the other minerals in Q4 and Q5,

respectively. The range in the respective mineral values is also distinctly higher than in the other classes. Little correlation is evident between the smectite-containing

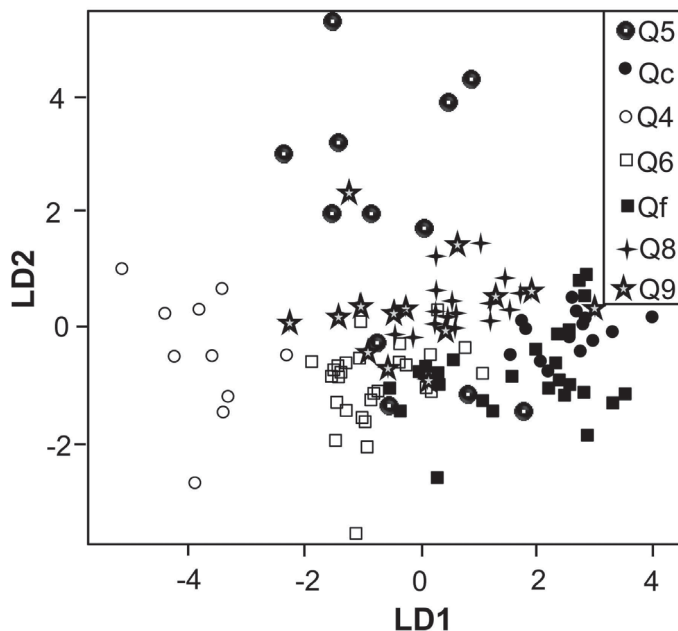


Figure 9. Scatter plot of LD1 and LD2 results at the quarry level.

Table 5. Summary statistics for predictor minerals at the Epoch level. Values in wt.%.

Mineral predictor	Statistical parameters	Pliocene	M. Miocene	L. Miocene	U. Eocene	M. Eocene
Quartz	min	2.0	2.9	2.2	1.2	1.7
	max	8.6	5.7	4.6	11.4	11.2
	median	6.5	4.3	2.6	3.2	5.5
	q1	2.8	2.9	2.3	2.4	5.1
	q3	7.8	4.8	3.2	5.1	7.5
Fe-rich smectite	min	5.0	6.0	29.9	7.2	4.8
	max	21.6	10.4	45.0	34.2	32.8
	median	9.8	8.7	37.8	21.1	14.8
	q1	5.7	8.3	34.6	13.6	10.8
	q3	21.0	9.7	41.3	29.5	17.9
Coarsely crystalline kaolinite	min	4.2	14.3	4.6	12.2	8.7
	max	9.7	21.7	10.4	25.5	18.3
	median	8.2	18.1	8.4	17.2	14.2
	q1	7.0	16.2	6.9	15.7	11.6
	q3	8.7	21.2	9.1	20.7	15.6
Fe-poor I-S	min	17.4	10.8	7.8	4.9	13.1
	max	36.0	20.2	22.8	20.9	22.7
	median	28.3	14.1	16.6	12.2	19.2
	q1	19.2	13.0	10.5	8.9	16.4
	q3	35.7	14.9	20.5	15.3	20.8
Illite	min	5.3	1.2	2.2	0.0	1.9
	max	12.6	5.7	8.3	5.5	8.0
	median	6.6	3.6	4.2	3.3	3.9
	q1	5.7	3.0	3.3	1.5	3.3
	q3	12.2	4.8	5.1	3.8	4.3

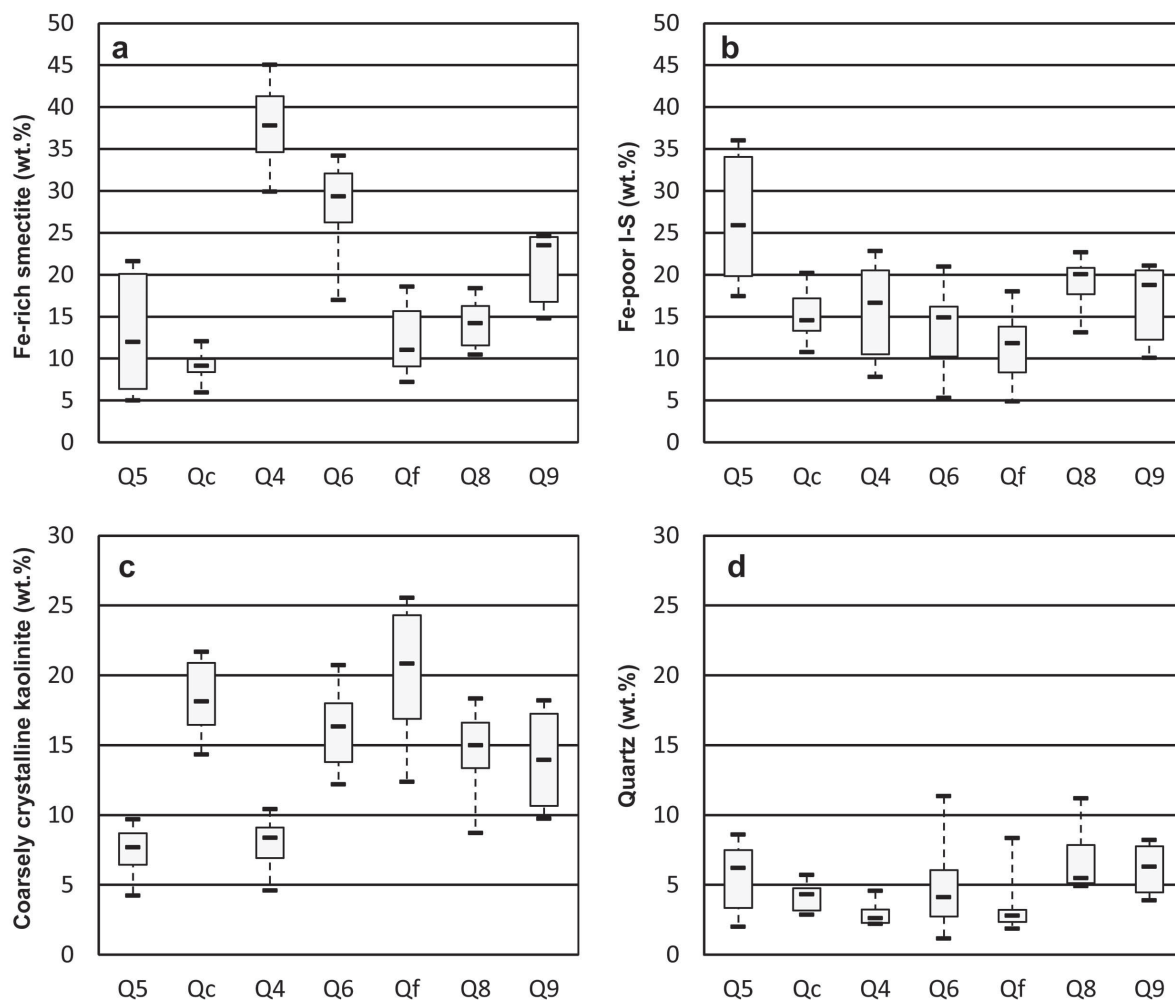


Figure 10. Boxplot of XRD predictor-mineral abundances in each quarry based on class assignments derived from a modified DFA model. Values are given in Table 6.

samples and the coarsely crystalline kaolinite (Figure 10c). As at the other levels of investigation, quartz is generally the least abundant of the predictors and exhibits considerable overlap of values for the different classes (Figure 10d).

Summary of DFA results

The statistical analysis succeeded in recognizing significant mineralogical differences among the Egyptian bentonitic clay samples on a regional scale (province), by age (Epoch), and by site (quarry). Based on previously classified samples, the probability of correctly assigning a sample at the province level was 92%, 78% at the Epoch level, and 75.4% at the quarry level when only the highest probability determinants of class were considered. The success rate increased to >94% when the second-highest probability choices were included. A test of five new, blind samples indicated that the probability of making the correct assignment to the

quarry of origin was 80%. The most important XRD predictor variables were Fe-rich smectite, coarsely crystalline kaolinite, Fe-poor I-S, and less frequently illite and quartz. Two other XRD predictor variables, S-moderate I-S, and KAOL2 were not important contributors to the three most heavily weighted linear discrimination functions at each level of classification. Seven of the 14 measured XRD mineral abundances could be excluded from the DFA due to their correlation with other predictors, or their highly skewed (non-normal) distribution. The reduction in the number of variables made it easier to determine differences in mineral content that occur on the region, age, and quarry levels.

DISCUSSION

A DFA of the XRD-determined mineralogical content of Egyptian bentonitic clays established an empirical basis for the separation and classification of samples that

Table 6. Summary statistics for predictor minerals at the quarry level. Values are in wt.%.

Mineral predictor	Statistical parameters	Q5	Qc	Q4	Qf	Q6	Q8	Q9
Fe-rich smectite	min	5.0	6.0	29.9	7.2	17.0	10.4	14.8
	max	21.6	12.0	45.0	18.6	34.2	18.4	24.6
	median	12.0	9.1	37.8	11.0	29.3	14.2	23.5
	q1	6.4	8.4	34.6	9.1	26.3	11.6	16.8
	q3	20.1	9.9	41.3	15.7	32.1	16.3	24.5
Coarsely crystalline kaolinite	min	4.2	14.3	4.6	12.4	12.2	8.7	9.7
	max	9.7	21.7	10.4	25.5	20.7	18.3	18.2
	median	7.7	18.1	8.4	20.8	16.3	15.0	13.9
	q1	6.4	16.5	6.9	16.9	13.8	13.4	10.7
	q3	8.7	20.9	9.1	24.3	18.0	16.6	17.3
Fe-poor I-S	min	17.4	10.8	7.8	4.9	5.3	13.1	10.1
	max	36.0	20.2	22.8	18.0	20.9	22.7	21.1
	median	25.9	14.5	16.6	11.8	14.9	20.1	18.8
	q1	19.8	13.3	10.5	8.4	10.2	17.7	12.3
	q3	34.1	17.2	20.5	13.8	16.2	20.8	20.5
Quartz	min	2.0	2.9	2.2	1.9	1.2	4.9	3.9
	max	8.6	5.7	4.6	8.3	11.4	11.2	8.2
	median	6.2	4.3	2.6	2.8	4.1	5.5	6.3
	q1	3.4	3.2	2.3	2.3	2.7	5.1	4.5
	q3	7.5	4.8	3.2	3.2	6.1	7.8	7.8

Qc = Q1 + Q2 + Q3; Qf = Q7 + Q12

were successful at the 94–100% level based on first and second highest probabilities for back-classification of the samples in the training set and 80% successful in classifying blind samples at the quarry level. The goals to classify samples at the province (mining district), age, and quarry levels, and to identify the mean mineral content of the classes were achieved. The assignment to class based on probability estimates of membership is a major advantage of DFA.

The reduction in the number of components in the XRD results from 14 to 5 established the roles of Fe-rich smectite, Fe-poor I-S, coarsely crystalline kaolinite, illite, and quartz as predictor minerals, and made it easier to identify the important compositional differences due to province (mining district), age, and in individual quarries. Changes in the abundances of the XRD predictors are statistically significant. In Egypt, differences are observed in the clays of different ages from different quarry locations and geographic provinces.

Misclassification of samples is the most frequently encountered problem in the use of DFA and usually results from errors due to the incorrect assignment of a sample to one of the *a priori* classes, mistakes in laboratory procedures, or small-scale stratigraphic variation which field-sample replication does not identify. In extreme cases, the errors may prevent closure of the analysis. Attention to stratigraphic details during sample collection and quality-control procedures in the laboratory will minimize the occurrences. When problems are

suspected, or simply to understand the sample variation, the original training set can be purified to eliminate problematic sample results and improve the classification. Procedures are also available to identify outliers so that they may be excluded from the training data (Hadi, 1992).

All of DFA, cluster, factor, and PCA seek to define those associations of variables that define unique groups (classes). The DFA has its strength in the fact that the populations (classes) are known from knowledge of the geology and characteristics of the samples. In cases where the starting point is a dataset with unknown classes, the classes established by cluster, factor, and principal-components analysis can be improved and consolidated by later applying DFA. As the results of a DFA are given in terms of probability of membership in a given class, the decision based on multivariate statistical procedures is presented in terms ranging from most likely to least likely. The method provides a logical and empirical basis for decisions regarding the similarities or differences amongst samples. The reliability of DFA in general has been established in a large number of publications over the past 30 y (*e.g.* Johnson and Winchern, 2007).

The DFA results can be used in the exploration and exploitation of bentonite deposits. In the simplest case, sample results from exploratory programs could be matched with existing quarry data to determine their similarity to materials in existing quarries. A match would suggest that the new materials could be used for

the same purposes. Alternatively, the XRD pattern from a sample with known desirable properties from a distant source could be processed to determine which Egyptian quarry is likely to be a new, local source for the clay.

Detailed XRD procedures based on structural and chemical details are important sources of basic data for the DFA. The use of simulated clay patterns allows the recognition of species that are more specific with regard to a particular clay mineral rather than simply assigning the clay peaks to broad groups such as smectite, mixed-layered clay minerals, or kaolinite. Samples with different quantities of clay mineral species will have distinct geologic origins and industrial uses. The Fe-rich smectite with little mixed layering may be the end product of submarine alteration of volcanic glasses or pedogenesis in vertisols (Clauer *et al.*, 1990; Zhang *et al.*, 1998; Cuadros *et al.*, 1999; Shoal, 2004). Samples with abundant Fe-rich smectite should have the largest surface areas and cation-exchange capacities. The randomly interlayered I-S with 60% smectite layers is most likely to have formed from the weathering of a mica precursor as burial diagenetic conditions had not been achieved. Coarsely crystalline kaolinite, distinguished from finely crystalline kaolinite, is indicative of more advanced crystal growth that could reflect intensity of weathering in the source terrane. Another major factor affecting differences in the clay content is segregation of detrital clay minerals during transport and deposition, or variable quantities of terrestrial input (Gibbs, 1977; Bolle *et al.*, 2000).

'Grade' is an informal comparative term dependent on smectite content and sample purity that is used to indicate the potential uses for a bentonite. An index of grade, the S/K ratio, can be obtained by dividing the sum of all smectite-containing phase abundances (Fe-rich smectite plus the three I-S phases) by the total for all kaolinites. S/K provides a measure of smectite abundance relative to the most abundant contaminant, kaolinite. Three quarries have a mean index of >2.0 , six have ratios near 0.5, and three are between 1.0 and 2.0 (Figure 11). Quarries Q4, Q5, and Q10 contain the highest-grade clays. They represent the highest-purity bentonite samples to test for use in specific applications such as drilling muds, pet litter, foundry and binding sands, pharmaceuticals, pelletizing, or cements (Chang, 2002). The presence of calcite in Q10 may lead to difficulties in applications based on acid activation such as oil clarification, or other processes causing calcite dissolution. The presence of moderately high kaolinite contents generally restricts the uses of many of these bentonites.

CONCLUSIONS

The XRD analyses revealed that all the quarries contain Fe-rich dioctahedral smectite, kaolinite (three varieties with different crystallite sizes), smectite-illite

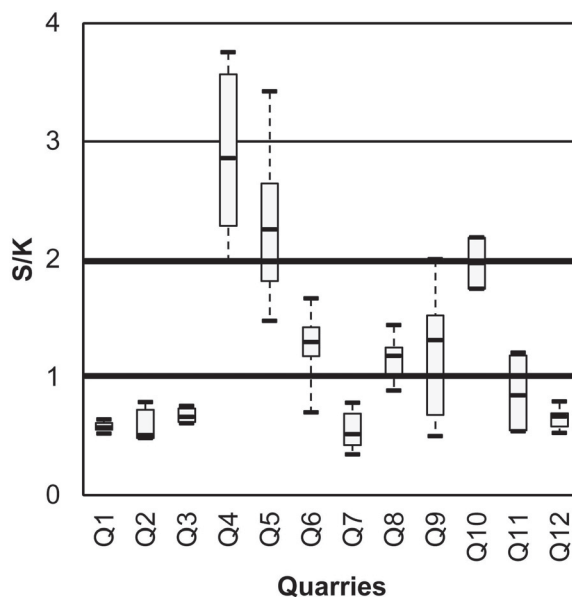


Figure 11. Box plot of smectite/kaolinite (S/K) abundance ratios in all 12 quarries. Horizontal lines separate locations with high-grade use potential ($S/K > 2$) from those with more limited applicability ($S/K < 1$).

mixed-layer minerals (three randomly interlayered varieties with 60, 70, or 80% Fe-poor smectite layers), illite, quartz, and feldspars. Some contain gypsum and calcite. The most abundant minerals are the smectitic and kaolinite minerals; while illite and non-clay minerals are least abundant. Discriminant function analysis indicated that the three most reliable XRD predictors of membership in a given class (province, Epoch, or quarry) are Fe-rich smectite, Fe-poor illite/smectite with 0.6 expandable layers, and coarsely crystalline kaolinite, followed by illite and quartz. The abundance of kaolinite varieties may restrict the utility of bentonites from certain quarries.

After an Aitchison's (1986) simple log-ratio transformation of the data, the DFA was able to classify an individual sample with respect to province, Epoch, and quarry with a certainty that the first choice selected by the program was correct 75–92% of the time. Including the second choice, the predictability exceeded 94%. The DFA is also very useful in grouping unknown samples into the various classes, particularly at the quarry level, that should be an aid in the correlation and exploitation of bentonitic clay deposits in the region. The results form a unique mineralogical database the members of which can be distinguished by multivariate statistical procedures.

ACKNOWLEDGMENTS

This investigation was part of a PhD dissertation funded by a joint supervision program, Egyptian Cultural Affairs and Missions Sector. Assistance with fieldwork was provided by Dr Ali Abdel-Motelib (Cairo University)

and Dr Sobhi Helal (Fayoum University). M.A. is grateful to Prof. Dr Ahmed G. Shedeed and Dr Mohamed Abu El-Ghar (Fayoum University) for making his work in Egypt possible. Wanda LeBlanc assisted ably in all phases of laboratory work at Louisiana State University (LSU). Many thanks to Andy Harrison and Nchekwube Mbmalu, former LSU graduate students, for their help with interpretation of the data. The LSU Department of Geology & Geophysics provided support for the project.

REFERENCES

- Abdel-Motelib, A., Kader, Z.A., Ragab, Y.A., and Mosalamy, M. (2011) Suitability of a Miocene bentonite from North Western Desert of Egypt for pharmaceutical use. *Applied Clay Science*, **52**, 140–144.
- Abu El Ezz, A.R., Kholeif, M.M., and Abdo, A.A. (1993) Contribution to mineralogy and geochemistry of some bentonite deposits in Egypt. *El-Minia Science Bulletin*, **6**, 79–88.
- Agha, M.A., Ferrell, R.E., Hart, G.F., Abu El Ghar, M.S., and Abdel-Motelib, A. (in revision) Mineralogy of Egyptian bentonitic clays II: Geologic origin.
- Aitchison, J. (1986) *The Statistical Analysis of Compositional Data*. Chapman & Hall, London, UK, 416 pp.
- Alberti, A. and Brigatti, M.F. (1985) Crystal chemical differences in Al-rich smectites as shown by multivariate analysis of variance and discriminant analysis. *Clays and Clay Minerals*, **33**, 546–548.
- Aparicio, P. and Ferrell, R.E. (2001) An application of profile fitting and CLAY++ for the quantitative representation (QR) of mixed-layer clay minerals. *Clay Minerals*, **36**, 501–514.
- Bailey, S.W. (1982) Nomenclature for regular inter-stratifications: *American Mineralogist*, **67**, 394–398.
- Barbera, G., Lo Guidice, A., Mazzoleni, P., and Pappalardo, A. (2009) Combined statistical and petrological analysis of provenance and diagenetic history of mudrocks: Application to Alpine Tethydean shales (Sicily, Italy). *Sedimentary Geology*, **213**, 27–40.
- Bertog, J., Huff, W., and Martin, J.E. (2007) Geochemical and mineralogical recognition of the bentonites in the lower Pierre Shale Group and their use in regional stratigraphic correlation. In: *The Geology and Paleontology of the Late Cretaceous Marine Deposits of the Dakotas* (J.E. Martin and D.C. Parris, editors). Geological Society of America Special Paper **427**, pp. 23–50.
- Bolle, M.P., Pardo, A., Adatte, T., Von Salis, K., and Burns, S. (2000) Climatic evolution on the southeastern margin of the Tethys (Negev, Israel) from the Paleocene to the early Eocene: focus on the late Paleocene thermal maximum. *Journal of the Geological Society of London*, **157**, 929–941.
- Chang, L.L.Y. (2002) *Industrial Mineralogy: Materials, Processes, and Uses*. Prentice Hall, New Jersey, USA, 472 pp.
- Chayes, F. (1960) On correlation between variables of constant sum. *Journal of Geophysical Research*, **65**, 4185–4193.
- Christidis, G.E. (2001) Geochemical correlation of bentonites from Milos Island, Aegean, Greece. *Clay Minerals*, **36**, 295–306.
- Clauer, N., O'Neil, J.R., Bonnot-Courtois, C., and Holtzappel, T. (1990) Morphological, chemical and isotopic evidence for an early diagenetic evolution of detrital smectite in marine sediments. *Clays and Clay Minerals*, **38**, 33–46.
- Cuadros, J., Caballero, E., Huertas, F.J., De Cisneros, C.J., Huertas, F., and Linares, J. (1999) Experimental alteration of volcanic tuff: smectite formation and effect on ¹⁸O isotope composition. *Clays and Clay Minerals*, **47**, 769–776.
- Cook, H.E., Johnson, P.D., Matti, J.C., and Zemmels, I. (1975) Methods of sample preparation and X-ray diffraction data analysis. *Initial reports of the Deep Sea drilling project, Riverside, California, University of California*, **28**, 999–1007.
- Cravero, F., Marfil, S.A., and Maiza, P.J. (2010) Statistical analysis of geochemical data: a tool for discriminating between kaolin deposits of hypogene and supergene origin, Patagonia, Argentina. *Clay Minerals*, **45**, 183–196.
- Daunis-I-Estadella, J., Barcelo-Vidal, C., and Buccianti, A. (2006) Exploratory compositional data analysis. Pp. 161–174 in: *Compositional Data Analysis in the Geosciences: From Theory to Practice* (A. Buccianti, G. Mateu-Figueras and V. Pawlowsky, editors). Special Publication **264**, Geological Society, London.
- Eden, D.N., Palmer, A.S., and Cronin, S.J. (2001) Dating the culmination of river aggradation at the end of the last glaciation using distal tephra compositions, eastern North Island, New Zealand. *Geomorphology*, **38**, 133–151.
- Eggleton, R.A. (1977) Nontronite: chemistry and X-ray diffraction. *Clay Minerals*, **12**, 181–194.
- Eisenhour, D.D. and Brown, R.K. (2009) Bentonite and its impact on modern life. *Elements*, **5**, 83–88.
- Ekosse, G-I.E. and Mwitondi, K.S. (2009) Multiple data clustering algorithms applied in search of patterns of clay minerals in soils close to an abandoned manganese oxide mine. *Applied Clay Science*, **46**, 1–6.
- Ferrell, R.E. (2006) *Clay Mineralogy: Introductory Course Material on a CD. E-Series 1*, The Clay Minerals Society, Chantilly, Virginia, USA.
- Ferrell, R.E. and Dypvik, H. (2009) The mineralogy of the Exmore beds – Chickahominy Formation boundary section of the Chesapeake Bay impact structure revealed in the Eyreville core. *Geological Society of America Special Paper*, **458**, pp. 723–746.
- Ferrell, R.E., Hart, G.F., Swamy, S., and Murthy, B. (1998) X-ray mineralogy discrimination of depositional environments of the Krishna Delta, Peninsular India. *Journal of Sedimentary Research*, **68**, 148–154.
- Galán, E. (2006) Genesis of clay minerals. Pp. 1129–1162 in: *Handbook of Clay Science* (F. Bergaya, B.K.G. Theng, and G. Lagaly, editors). Elsevier, Oxford, UK.
- Galán, E., Aparicio, P., Gonzalez, I., and Miras, A. (1998) Contribution of multivariate analysis to the correlation of some properties of kaolin with its mineralogical and chemical composition. *Clay Minerals*, **33**, 65–75.
- Gibbs, R.J. (1977) Clay mineral segregation in the marine environment. *Journal of Sedimentary Petrology*, **47**, 243–273.
- Grim, R.E. and Guven, N. (1978) *Bentonites: Geology, Mineralogy, Properties and Uses*. Developments in Sedimentology, **24**, Elsevier North-Holland, Amsterdam, 256 pp.
- Hadi, A.S. (1992) Identifying multiple outliers in multivariate data. *Journal of the Royal Statistical Society, Series B*, **54**, 761–771.
- Hart, G.F. (1994) Maceral palynofacies of the Louisiana deltaic plain in terms of organic constituents and hydrocarbon potential. Pp. 141–176 in: *Sedimentation of Organic Particles* (A. Traverse, editor). Cambridge University Press, Cambridge, UK.
- Hart, G.F. (2011a) eNote00. Transformation of variables for compositional data-analysis. 17 pp. (<http://www.geol.lsu.edu/hart/eNotes/eNotes.html>, accessed 23 June 2012).
- Hart, G.F. (2011b) eNote01. Error checking of the mineralogical data-frame: Bentonite Quarry study of Egypt. 128 pp. (<http://www.geol.lsu.edu/hart/eNotes/eNotes.html>, accessed 23 June 2012).
- Hart, G.F., Ferrell, R.E., Lowe, D.R., and Lenoir, A.E. (1989) Shelf sandstones of the *Robulus* L zone, offshore Louisiana.

- Pp. 117–141 in: *Shelf Sedimentation, Shelf Sequences and Related Hydrocarbon Accumulation* (R.A. Morton and D. Nummedal, editors). Proceedings of the Seventh Annual Gulf Coast Section SEPM Research Conference.
- Hassan, M.S. and Abdel-Khalek, N.A. (1998) Beneficiation and applications of an Egyptian Bentonite. *Applied Clay Science*, **13**, 99–115.
- Huff, W.D. and Kolata, D.R. (1990) Correlation of K-bentonite beds by chemical fingerprinting using multivariate statistics. Pp. 567–577 in: *Quantitative Dynamic Stratigraphy* (T.A. Cross, editor). Prentice Hall, New Jersey, USA.
- Huff, W.D., Bergstrom, S.M., and Kolata, D.R. (2010) Ordovician explosive volcanism. In: *The Ordovician Earth System*. Geological Society of America Special Paper, **466**, pp. 13–28.
- Ingelthorpe, S.D.J., Morgan, D.J., Hegley, D.E., and Bloodworth, A.J. (1993) *Industrial Minerals Laboratory Manual* “Bentonite”. Technical Report WG/93/20, Mineralogy and Petrology Group, British Geological Survey, UK.
- Johnson, R.A. and Winchurn, D.W. (2007) *Applied Multivariate Statistical Analysis* (6th edition). Prentice Hall, New Jersey, USA.
- Kiipli, T., Kallaste, T., Nestor, V., and Loydell, D.K. (2010) Integrated Telychian (Silurian) K-bentonite chemostratigraphy and biostratigraphy in Estonia and Latvia. *Lethaia*, **43**, 32–44.
- Kolata, D.R., Huff, W.D., and Bergstrom, S.M. (1996) Ordovician K-bentonites of Eastern North America. *Geological Society of America Special Paper*, **313**, 84 pp.
- Martin-Fernandez, J.A. and Thio-Henestrosa, S. (2006) Rounded zeros: some practical aspects for compositional data. Pp. 191–201 in: *Compositional Data Analysis in the Geosciences: From Theory to Practice* (A. Buccianti, G. Mateu-Figueras, and V. Pawlowsky, editors). Special Publication, **264**, Geological Society, London.
- Moebis, A., Cronin, S.J., Neall, V.E., and Smith, I.E. (2011) Unravelling a complex volcanic history from fine-grained, intricate Holocene ash sequences at the Tongariro Volcanic Centre, New Zealand. *Quaternary International*, **246**, 352–363.
- Montero-Serrano, J.C., Pararea-Albaladejo, J., Martin-Fernandez, J.A., Martinez-Santana, M., and Gutierrez-Martin, J.V. (2010) Sedimentary chemofacies characterization by means of multivariate analysis. *Sedimentary Geology*, **228**, 218–228.
- Moore, D.M. and Reynolds, R.C. (1989) *X-ray Diffraction and the Identification and Analysis of Clay Minerals*. Oxford University Press, Oxford, UK, 332 pp.
- Murray, H.H. (2007) *Applied Clay Mineralogy: Occurrences, Processing and Applications of Kaolins, Bentonites, Palygorskite-Septiolite, and Common Clays*. Developments in Clay Science, **2**, Elsevier, Amsterdam, 188 pp.
- Odom, I.E. (1984) Smectite clay minerals: properties and uses. *Philosophical Transactions of the Royal Society of London*, **311** 391–332.
- Petschick, R. (2004) *MacDiff* 4.2.5. Power Diffraction Software: (<http://www.geologie.uni-frankfurt.de/staff/Homepages/Petschick/MacDiff/MacDiffInfoE.html>, accessed 23 June 2012).
- Prudencia, M.I., Sequeira Braga, M.A., Oliviera, F., Dias, M.I., Delgado, M., and Martins, M. (2006) Raw material sources for the Roman Bracaraense ceramics (NW Iberian Peninsula). *Clays and Clay Minerals*, **54**, 638–649.
- R statistical package version 2.10.1 (2009) The R Foundation for Statistical Computing. ISBN 3-900051-07-0.
- Sanchez, C. and Galán, E. (1995) An approach to the genesis of palygorskite in a Neogene–Quaternary continental basin using principal factor analysis. *Clay Minerals*, **30**, 225–238.
- Shane, P.A.R. and Froggatt, P.C. (1994) Discriminant function analysis of glass chemistry of New Zealand and North American tephra deposits. *Quaternary Research*, **41**, 70–81.
- Shapiro, S.S. and Wilk, M.B. (1965) An analysis of variance test for normality (complete samples). *Biometrika*, **52**, 591–611.
- Shoval, S. (2004) Deposition of volcanogenic smectite along the southeastern Neo-Tethys margin during the oceanic convergence stage. *Applied Clay Science*, **24**, 299–311.
- Środoń J. (2006) Identification and quantitative analysis of clay minerals. Pp. 765–787 in: *Handbook of Clay Science* (F. Bergaya, B.K.G. Theng, and G. Lagaly, editors). Developments in Clay Science, **1**. Elsevier, Amsterdam.
- Varadachari, C. and Mukherjee, G. (2004) Discriminant analysis of clay mineral compositions. *Clays and Clay Minerals*, **52**, 311–320.
- von Eynatten, H., Barcelo-Vidal, C., and Pawlowsky-Glahn, V. (2003) Sandstone composition and discrimination: a statistical evaluation of different analytical methods. *Journal of Sedimentary Research*, **73**, 47–57.
- Weltje, G.J. (2002) Quantitative analysis of detrital modes: statistically rigorous confidence regions in ternary diagrams and their use in sedimentary petrology. *Earth-Science Reviews*, **57**, 211–253.
- Zhang, L., Sun, M., Wang, S., and Yu, X. (1998). The composition of shales from the Ordos basin, China: effects of source weathering and diagenesis. *Sedimentary Geology*, **116**, 129–141.

(Received 31 August 2011; revised 18 August 2012; Ms. 611; AE: S. Kadir)